Cosmological constraints from baryon acoustic oscillations and clustering of large-scale structure

G. E. Addison^{1*}, G. Hinshaw¹ and M. Halpern¹
¹Department of Physics and Astronomy, University of British Columbia, 6224 Agricultural Road, Vancouver, BC V6T 1Z1, Canada

Accepted xxx. Received xxx; in original form xxx

ABSTRACT

We constrain cosmological parameters using combined measurements of the baryon acoustic oscillation (BAO) feature in the correlation function of galaxies and Ly- α absorbers that together cover 0.1 < z < 2.4. The BAO position measurements alone – without fixing the absolute sound horizon 'standard ruler' length with cosmic microwave background (CMB) data – constrain $\Omega_m=0.303\pm0.040$ (68 per cent confidence) for a flat $\Lambda {\rm CDM}$ model, and $w=-1.06^{+0.33}_{-0.32}, \Omega_m=0.292^{+0.045}_{-0.040}$ for a flat wCDM model. Adding other large-scale structure (LSS) clustering constraints – correlation function shape, the Alcock-Paczynski test and growth rate information – to the BAO considerably tightens constraints ($\Omega_m = 0.290 \pm 0.019$, $H_0 = 67.5 \pm 2.8 \text{ km s}^{-1} \text{ Mpc}^{-1}, \sigma_8 = 0.80 \pm 0.05 \text{ for } \Lambda\text{CDM}, \text{ and } w = -1.14 \pm 0.19 \text{ for } \Lambda\text{CDM}$ wCDM). The LSS data mildly prefer a lower value of H_0 , and a higher value of Ω_m , than local distance ladder and type IA supernovae (SNe) measurements, respectively. While tension in the combined CMB, SNe and distance ladder data appears to be relieved by allowing w < -1, this freedom introduces tension with the LSS σ_8 constraint from the growth rate of matter fluctuations. The combined constraint on w from CMB, BAO and LSS clustering for a flat wCDM model is $w = -1.03 \pm 0.06$.

Key words: cosmological parameters – large-scale structure of Universe

INTRODUCTION

Recent measurements of temperature anisotropy in the cosmic microwave background (CMB) continue to strongly support the standard ACDM cosmological model, and now constrain its parameters to one or two per cent (e.g. Hinshaw et al. 2012; Story et al. 2012; Sievers et al. 2013; Planck Collaboration XVI 2013). While upcoming polarization data may yield insight into the physics of the early universe, with the recent release of Planck cosmology results, future improvements in ΛCDM constraints from the CMB will be modest. In the coming years, the precision of low-redshift cosmological constraints will significantly increase relative to those from the CMB, predominantly due to intensive efforts to constrain the evolution of dark energy (DE; e.g. Albrecht et al. 2006; Weinberg et al. 2012).

One powerful low-redshift probe is the measurement of position of the baryon acoustic oscillation (BAO) feature in the correlation function of large-scale structure (LSS), the imprint of sound waves in the pre-recombination plasma. The BAO measurements are one of the few low-redshift cosmological probes that are limited by statistical, rather than systematic, uncertainties (e.g. Weinberg et al. 2012, and references therein).

The BAO scale observed in LSS correlations is intimately related to the photon acoustic scale measured with high precision in

the CMB fluctuations (Eisenstein et al. 1998). Typically, BAO constraints are discussed, and compared with other low-redshift measurements, using CMB data to fix or tightly constrain portions of parameter space. In this work, we consider an alternative approach, and examine cosmological constraints from the latest BAO (and associated LSS clustering) measurements without strong CMB-based priors.

CMB and low-redshift measurements are subject to different observational issues and challenges, and affected differently by, for instance, any non-standard early-universe physics or late-time expansion. A hypothetical deviation from Λ -acceleration may first appear as a tension between CMB and low-redshift data, or between different low-redshift probes. Such tension in general could also arise from statistical fluctuations, systematic uncertainties that are incorrectly quantified, alternative extensions to the standard model, or some combination of these factors. The ability to disambiguate these possibilities is crucial if we are to get the most out of data from current and future low-redshift experiments. Already, mild tensions have been reported between BAO and local distance ladder measurements of H_0 in the context of a Λ CDM model, when analysed in conjunction with CMB data (e.g. Anderson et al. 2012; Hou et al. 2012; Planck Collaboration XVI 2013). We will show that there is now evidence for mild BAO-distance ladder tension even without calibrating the BAO measurements using the CMB constraint on the acoustic scale. Similarly, current BAO and LSS precision is now sufficient to permit a meaningful comparison with type IA supernovae (SNe) measurements of the low-redshift expansion rate without strong CMB priors. We show that the BAO and LSS data mildly prefer a higher matter density, Ω_m , than a recent SNe compilation.

The Λ CDM tensions between the CMB and distance ladder or SNe measurements reported by *Planck* (Planck Collaboration XVI 2013) are both effectively relieved by allowing the dark energy equation of state w < -1. We will show, however, that reducing w below -1 introduces some tension with the amplitude of matter fluctuations, σ_8 , measured using growth rate constraints from redshift-space distortions.

We anticipate that comparing results from different lowredshift probes, both together, and separately from, CMB constraints, will prove increasingly useful as data precision continues to improve.

In Section 2 we discuss the physical information provided by BAO measurements; Section 3 deals with our choice of data and fitting methodology; results are presented in Section 4, and a discussion and conclusions follow in Sections 5 and 6.

COSMOLOGY FROM THE BARYON ACOUSTIC OSCILLATION SCALE

The BAO feature in the LSS correlation function is the consequence of acoustic waves in the pre-recombination baryon – photon plasma, caused by the opposing forces of gravity and radiation pressure (Peebles & Yu 1970). A characteristic scale, roughly the distance these waves have propagated prior to recombination, is imprinted into the matter correlation function when baryons and photons decouple. This scale is typically called the sound horizon and is given by (Hu & Sugiyama 1996; Eisenstein & Hu 1998)

$$r_s = \int_{z_{\rm dras}}^{\infty} \frac{c_s(z)}{H(z)} dz, \tag{1}$$

where $z_{
m drag}$ is the redshift at which baryons ceased to be influenced by Compton drag from photons, $c_s = c/\sqrt{3(1+R)}$ is the sound speed, a function of the ratio of baryon and photon momentum densities, $R = 3\rho_b/4\rho_\gamma$. In order to be consistent with existing BAO analyses, we adopt the definitions, and fitting formulae for $z_{\rm drag}$, from Eisenstein & Hu (1998). For the cosmologies we consider, rescaling a numerical calculation of z_{drag} from the CAMB distribution (Lewis et al. 2000), as in Hou et al. (2012) and Planck Collaboration XVI (2013), changes the inferred BAO constraints by less than 0.2 per cent¹ compared to our treatment, which is a negligible difference for current BAO precision.

Studies based on catalogues of LSS tracers measure separations in the radial (line-of-sight; redshift) and transverse (angular) directions. The observables corresponding to the BAO scale are $\Delta z = H(z) r_s/c$ and $\Delta \theta = r_s/(1+z)D_A$, respectively, where D_A is the comoving angular diameter distance. Constraints are typically reported in terms of these quantities or D_V/r_s , where D_V is a combination of radial and transverse distances (Eisenstein et al. 2005):

$$D_V(z) = \left[(1+z)^2 D_A^2(z) \frac{cz}{H(z)} \right]^{1/3}.$$
 (2)

moving Mpc, means the BAO feature remains identifiable in lowredshift LSS despite the effects of non-linear growth of structure

The large size of the sound horizon, approximately 150 co-

(e.g. Tegmark 1997; Eisenstein et al. 2007b), however the contrast of the feature is fairly low, essentially because baryons represent a small fraction of the total matter density. Measuring BAO therefore requires surveys that sample large cosmological volumes. The BAO feature in the galaxy correlation function was first detected by the Sloan Digital Sky Survey (SDSS; Eisenstein et al. 2005) and Twodegree-Field Galaxy Redshift Survey (2dFGRS; Cole et al. 2005), and has subsequently also been measured using galaxy samples over 0 < z < 1 by the Six-degree-Field Galaxy Survey (6dFGS; Beutler et al. 2011), the WiggleZ Dark Energy Survey (Blake et al. 2011c), and the Baryon Oscillation Spectroscopic Survey (BOSS; Anderson et al. 2012).

Recently, the BAO feature has been measured in the correlation function of Lyman- α (Ly- α) absorbers at $2 \lesssim z \lesssim 3$ using sight-lines to BOSS quasars (Busca et al. 2013; Slosar et al. 2013). The Ly- α measurements are more sensitive to the BAO feature in the radial direction; we follow Busca et al. (2013) in using the constraint on the radial BAO scale relative to a fiducial model,

$$\alpha_r = \frac{[H(z) r_s]_{\text{fid}}}{H(z) r_s}.$$
 (3)

to constrain cosmological models.

Jointly considering the transverse and radial Ly- α constraints somewhat tightens constraints but does not impact qualitatively on our conclusions. Future Ly- α data may warrant a more detailed approach than we consider here.

2.1 Constraints from BAO position alone

Measurements of the BAO scale are sensitive to the low-redshift expansion rate through D_A and H(z), and so constrain Ω_m (with Ω_{Λ} determined implicitly in a flat ΛCDM model). A joint fit to BAO data over a range of redshift also constrains an overall normalisation that in this work we will express as the combination $H_0 r_s$. Going beyond the standard model, BAO measurements alone also constrain parameters that modify the low-redshift expansion rate, such as w. BAO-only constraints on Ω_m and w can be directly compared with those from, for instance, type IA SNe, without requiring an external constraint on the absolute 'standard ruler' scale r_s from CMB anisotropy. This comparison is now becoming meaningful owing to the addition of the high-redshift Ly- α BAO constraint to existing z < 1 BAO measurements.

It should be noted that we view the wCDM fits in this work as a mathematical exercise in expansion history parametrization - something like a ACDM null-test - and do not present or discuss any particular physical model that could give rise to $w \neq$ -1. We also do not investigate allowing additional freedom in w, for instance through the popular $w_0 - w_a$ parametrization (Chevallier & Polarski 2001; Linder 2003), since BAO measurements alone do not (yet) usefully constrain such additional parameters.

2.2 Additional constraints from LSS clustering

The clustering of LSS tracers contains cosmological constraints beyond simply the position of the BAO feature, although extracting this information typically requires somewhat stronger assumptions regarding the bias of the tracers or the underlying shape of the matter power spectrum. We here briefly review the additional constraints that we incorporate in the second stage of our analysis.

Marginalising over uncertainties in bias, one can use the entire measured power spectrum as a standard ruler, rather than just the BAO position feature (e.g. Eisenstein et al. 2005; Sánchez et al. 2008; Shoji et al. 2009). Blake et al. (2011c) used this approach to constrain the parameter $A_s = 100 D_V \sqrt{\Omega_m h^2}/cz$ from the overall power spectrum shape measured from WiggleZ. An additional constraint can be obtained by matching the transverse and radial clustering shapes (i.e. by enforcing statistical isotropy) – known as the Alcock-Paczynski (AP) test (Alcock & Paczynski 1979). This constrains the product of D_A and H, which can be expressed as, for example, $F(z) = (1+z)D_A(z)H(z)/c$. It is important to account for anisotropy from redshift-space distortion due to LSS tracer peculiar velocity (Kaiser 1987) when applying the AP test (Ballinger et al. 1996). Provided non-linearities can be robustly treated, the inclusion of redshift-space power spectrum data constrains $f(z)\sigma_8(z)$, where $f = d \ln \delta/d \ln a$ is the linear growth rate, and $\sigma_8(z) = \sigma_8[\delta(z)/\delta(0)]$, where σ_8 is the rms linear mass fluctuations in spheres of radius $8 h^{-1}$ Mpc at redshift zero.

The constraints on $\Omega_m h^2$ from the shape of the galaxy power spectrum (e.g. Eisenstein et al. 2005; Reid et al. 2010; Chuang & Wang 2013; Chuang et al. 2013) mean H_0 and r_s can be separately constrained. This is a powerful and useful feature because it allows constraints on H_0 from LSS clustering to be compared to other more direct H_0 measurements for a given cosmological model (Section 5.1). Similarly, the joint constraints on Ω_m and σ_8 can be compared with weak lensing and cluster counting analyses (Section 5.3).

When fitting the growth rate data in a wCDM model, we use the following expression for the linear growing mode solution, valid for a flat universe, which is assumed throughout this work (Silveira & Waga 1994)

$$\delta(z) = \frac{1}{1+z} \, {}_{2}F_{1} \left[-\frac{1}{3w}, \frac{w-1}{2w}, 1 - \frac{5}{6w}, -(1+z)^{3w} \frac{1-\Omega_{m}}{\Omega_{m}} \right], \tag{4}$$

where ${}_2F_1$ is the hypergeometric function.

3 DATA AND MODEL FITTING

The BAO data used in our analysis are listed in Table 1. We opt to use recent analyses of the SDSS Data Release (DR) 7 and BOSS DR9 CMASS samples that constrain the BAO position in both the radial and transverse directions (Xu et al. 2013; Anderson et al. 2013). We also use SDSS and CMASS constraints from analyses that attempt reconstruction of the linear density field (Eisenstein et al. 2007a). Earlier results (e.g. Eisenstein et al. 2005; Percival et al. 2010) are in good agreement with these newer analyses.

The bottom part of Table 1 lists constraints used in our expanded analysis, including correlation function shape, AP and growth rate measurements, in addition to BAO feature position. It should be noted that the SDSS and BOSS CMASS samples have been re-analyzed multiple times (e.g. Reid et al. 2010; Samushia et al. 2012; Padmanabhan et al. 2012; Anderson et al. 2012; Sánchez et al. 2013). Some choice of which constraints to adopt must therefore be made. Ideally, one would jointly fit to the 'raw' data – the correlation function or power spectrum measurements – from each sample, rather than to derived quantities such as D_V/r_s . The latter approach is, however, adequate for this work, since our conclusions are largely qualitative and relatively insensitive to the exact choice of constraint combination (although see comments on goodness-of-fit in Section 4.1).

Chuang et al. (2013) present a 'single probe' analysis of the BOSS CMASS data, jointly using BAO position, clustering shape

and redshift-space distortion information to extract cosmological constraints, independent of dark energy evolution model, with broad priors on parameters not well-constrained from their data. This work built upon earlier analysis using the SDSS sample at $z_{\rm eff}=0.35$ (e.g. Chuang & Wang 2013). We opt not to include constraints from the earlier work in all our fits since they were found to be somewhat more sensitive to, for example, the range of separation scales used in correlation function fitting, although we consider the effect of their inclusion in the context of LSS constraints on H_0 in Section 5.1.

The interdependence between BAO position and growth rate (Beutler et al. 2012) has not been quantified for the 6dFGS and so for the expanded LSS clustering analysis we choose to use only the BAO scale constraint, and similarly for the SDSS $z_{\rm eff}=0.35$ sample. We do not include growth rate constraints from surveys outside those used for the BAO-only fit. This is a slightly arbitrary choice, however the growth rate constraints from other surveys, including 2dFGRS (Hawkins et al. 2003), 2SLAQ (Ross et al. 2007), VVDS (Guzzo et al. 2008), and VIPERS (de la Torre et al. 2013), are statistically consistent with the constraints used here, and do not provide significant improvements for the models considered.

The WiggleZ and 6dFGS analyses fixed several parameters, including the baryon density and primordial power spectrum index, n_s , based on Wilkinson Microwave Anisotropy Probe (WMAP) constraints (Komatsu et al. 2011). We do not view these assumptions as likely to lead to either bias in inferred BAO constraints, or significant interdependence between CMB and BAO or LSS constraints for the Λ CDM and wCDM models discussed in this work. The WiggleZ and 6dFGS data sets constrain D_V/r_s or A_s to around 5 per cent. The sound horizon varies very weakly with $\Omega_b h^2$ for the cosmologies we consider $(r_s \propto (\Omega_b h^2)^{-0.13})$, and is, furthermore, constrained to better than 1.5 per cent by the CMB (Planck Collaboration XVI 2013). Eisenstein et al. (2005) found that the acoustic parameter, A_s , scales as $n_s^{-0.35}$ from fitting to SDSS data. Assuming this relation, shifting a WiggleZ A_s value by 0.5σ requires a 7σ shift in n_s (as inferred from current CMB data for either Λ CDM or wCDM). The high precision of CMB constraints essentially means that uncertainty in these parameters is subdominant to sample variance for the WiggleZ and 6dFGS data. Far weaker CMB-based assumptions can be, and are, adopted for the more precise BAO and LSS measurements from SDSS and BOSS.

Blake et al. (2011b) used clustering information on scales down to $k=0.3~h{\rm Mpc}^{-1}$ to extract the WiggleZ growth rate constraints. To check that uncertainties relating to non-linear effects on these scales are not significantly biasing our results, we repeated the BAO plus LSS fit with the WiggleZ constraints removed. While parameter constraints are degraded (by up to a factor of two in the case of σ_8), the shifts in the peaks of the marginalised parameter posterior probability distributions are small – at most around 20 per cent of a statistical standard deviation – for all parameters.

In order to fit cosmological parameters, we introduce a likelihood function

$$-2\ln \mathcal{L} = (\mathbf{x} - \mathbf{d})^T \mathbf{C}^{-1} (\mathbf{x} - \mathbf{d}) - 2\ln \mathcal{L}_{Lv\alpha}, \tag{5}$$

where x, d and C are the model predictions, mean data values and data covariance matrix of the 6dFGS, SDSS, WiggleZ and BOSS CMASS constraints (including covariance between different constraints from the same survey).

Slosar et al. (2013) report a non-Gaussian and asymmetric probability distribution for α_r from the BOSS Ly- α forest measurements. We add the 'top-hat' systematic uncertainty of ± 0.02

4 Addison, Hinshaw & Halpern

Table 1. Measurements of BAO position and large-scale clustering (LSS) clustering used in this analysis. The LSS clustering measurements include constraints on the acoustic parameter, A_s , the Alcock-Paczynski (AP) parameter, F, and the growth rate, $f\sigma_8$, as defined in Section 2. Note that, while some BAO constraints are included in the LSS data set, the BAO-only data are not a subset of the LSS data (see Section 4.1). Cosmological constraints from the BAO and LSS data are discussed in Sections 4 and 5.

Label	Survey	$z_{ m eff}$	Constraint	Reference
BAO-only	6dFGS	0.106	$r_s/D_V = 0.336 \pm 0.015$	Beutler et al. (2011)
	SDSS, DR7 ^a	0.35 0.35	$D_A/r_s = 6.875 \pm 0.246$ $Hr_s = (12895 \pm 1070) \; {\rm km \; s^{-1}}$	Xu et al. (2013)
	$\mathrm{Wiggle}\mathrm{Z}^b$	0.44 0.60 0.73	$r_s/D_V = 0.0916 \pm 0.0071$ $r_s/D_V = 0.0726 \pm 0.0034$ $r_s/D_V = 0.0592 \pm 0.0032$	Blake et al. (2011c)
	BOSS, DR9 CMASS ^c	0.57 0.57	$D_A(r_s^{ m fid}/r_s) = (1408 \pm 45) { m Mpc}$ $H(r_s/r_s^{ m fid}) = (92.9 \pm 7.8) { m km s^{-1} Mpc^{-1}}$	Anderson et al. (2013)
	BOSS, Ly- α forest d	2.4	α_r ; see text	Slosar et al. (2013)
LSS	6dFGS	0.106	$r_s/D_V = 0.336 \pm 0.015$	Beutler et al. (2011)
	SDSS, DR7 ^a	0.35 0.35	$D_A/r_s = 6.875 \pm 0.246$ $Hr_s = (12895 \pm 1070) \; {\rm km \; s^{-1}}$	Xu et al. (2013)
	${\rm Wiggle}Z^b$	0.44 0.60 0.73 0.44 0.60 0.73 0.44 0.60 0.73	$A_s = 0.474 \pm 0.034$ $A_s = 0.442 \pm 0.020$ $A_s = 0.424 \pm 0.021$ $F = 0.482 \pm 0.049$ $F = 0.650 \pm 0.053$ $F = 0.865 \pm 0.073$ $f\sigma_8 = 0.413 \pm 0.080$ $f\sigma_8 = 0.390 \pm 0.063$ $f\sigma_8 = 0.437 \pm 0.072$	Blake et al. (2012)
	BOSS, DR9 CMASS e	0.57 0.57 0.57 0.57	$H = (87.6 \pm 7.2) \mathrm{km} \mathrm{s}^{-1} \mathrm{Mpc}^{-1}$ $D_A = (1396 \pm 74) \mathrm{Mpc}$ $\Omega_m h^2 = 0.126 \pm 0.019$ $f\sigma_8 = 0.428 \pm 0.069$	Chuang et al. (2013)
	BOSS, Ly- α forest d	2.4	α_r ; see text	Slosar et al. (2013)

^a the SDSS DR7 post-reconstruction measurements of D_A/r_s and Hr_s are correlated with correlation coefficient 0.57

obtained by Slosar et al. (2013) based on the scatter between different fitting methods linearly to the statistical uncertainty estimates to give $\alpha_r = 0.987^{+0.055}_{-0.053}^{+0.096}_{-0.053}^{+0.143}_{-0.087}(\pm 1, 2 \text{ and } 3\sigma \text{ errors})$. We then construct a polynomial likelihood of the form

$$-2 \ln \mathcal{L}_{Ly\alpha} = \begin{cases} C_1 x^2 + D_1 x^3 + E_1 x^4 & \text{for } \alpha_r \leq 0.987 \\ C_2 x^2 + D_2 x^3 + E_2 x^4 & \text{for } \alpha_r > 0.987, \end{cases}$$

where $x=|\alpha_r^{\rm model}-0.987|$, and the constants $C_{1,2}$, $D_{1,2}$ and $E_{1,2}$ are determined by matching to the ± 1 , 2 and 3σ uncertainties in α_r . Our analysis is insensitive to exactly how the Ly- α likelihood is treated – assuming a purely Gaussian likelihood, for instance, does not have any significant impact on our results.

Busca et al. (2013) present an analysis of largely the same Ly- α sample used by Slosar et al. (2013), but with various differences

in data cuts and methodology (see Section 5.4 of Slosar et al. 2013). We discuss the effects of using the Busca et al. (2013) results rather than those of Slosar et al. (2013) in Section 5.1.

We explore parameter spaces using a Markov Chain Monte Carlo (MCMC) method, specifically the affine-invariant 'stretch step' ensemble sampler proposed by Goodman & Weare (2010) and parallelised in the emcee² Python module by Foreman-Mackey et al. (2013). For the relatively small number of parameters we consider here, a tuned Metropolis sampler (Metropolis et al. 1953; Dunkley et al. 2005) would likely be more efficient, however we expect that the flexibility and parallel nature of the stretch step approach (above references and Akeret et al.

^b the covariance matrix for the WiggleZ measurements is given in equation (4) of Hinshaw et al. (2012) for D_V/r_s and Table 2 of Blake et al. (2012) for A_s , F and $f\sigma_8$

 $[^]c$ the BOSS DR9 CMASS sample post-reconstruction measurements of $D_A(r_s/r_s^{\rm fid})$ and $H(r_s/r_s^{\rm fid})$ are correlated with correlation coefficient 0.55; the fiducial sound horizon, $r_s^{\rm fid}$, adopted by Anderson et al. (2013) is $r_s^{\rm fid}=153.19$ Mpc

 $[^]d$ the fiducial value of $H\,r_s$ (equation 3) adopted for the BOSS Ly- α analysis is $3.62\times 10^4~{\rm km~s^{-1}}$

^e the covariance matrix between parameters in the full BOSS CMASS clustering analysis is given in equation (26) of Chuang et al. (2013)

² http://dan.iel.fm/emcee/

2012) to prove useful as we include more data sets in future analysis.

4 RESULTS

In this section we discuss constraints from the BAO-only and LSS clustering fits and compare to the latest CMB results. Here and throughout, 'CMB' refers to a joint fit to the *Planck* 2013 temperature and lensing power spectra (Planck Collaboration XV 2013; Planck Collaboration XVII 2013), *WMAP* 9-year polarization data (Bennett et al. 2012) and small-scale temperature power spectra from the Atacama Cosmology Telescope (ACT; Das et al. 2013) and the South Pole Telescope (SPT; Reichardt et al. 2012). We show constraints from MCMC chains provided by the *Planck* collaboration³. Comparisons with other data sets are made in Section 5

4.1 Λ**CDM**

For the Λ CDM fit to BAO position measurements alone we find $\Omega_m=0.304\pm0.040$ and $H_0\,r_s=(1.035\pm0.024)\times10^4$ km s $^{-1}$. We report mean parameter values and the boundaries of the symmetric 68.3 per cent and, in some cases, 95.5 per cent, confidence intervals. Constraints in the $H_0\,r_s-\Omega_m$ plane are shown in Figure 1 for the combined BAO data as well as the z=0.106 6dFGS, z=0.57 BOSS CMASS and z=2.4 BOSS Ly- α constraints individually. We show CMB constraints for the Λ CDM model in the same plane.

Our ΛCDM parameter space for the expanded LSS clustering fit is spanned by

$$\{\Omega_m, H_0, r_s, \sigma_8\}. \tag{7}$$

For the Λ CDM model, there is striking agreement for all parameters between the BAO-only, LSS, and CMB constraints (Table 2), consistent with the discussion in Section 5.2 of Planck Collaboration XVI (2013). Adding the LSS clustering information tightens constraints on Ω_m by a factor of two over the BAO position data alone, and constrains H_0 to around 4 per cent and σ_8 to around 6 per cent.

Notice that the LSS data contour in Figure 1 contains regions disfavoured in the BAO-only fit. This is because the strongest LSS constraints do not depend explicitly on the sound horizon, r_s . The BOSS CMASS and WiggleZ analyses used in the LSS fit (Blake et al. 2012; Chuang et al. 2013) focus on the shape of the galaxy correlation function – the dependence on r_s is effectively marginalised over in the case of Chuang et al. (2013), and negligible in the case of Blake et al. (2012), because the BAO feature is not significantly detected in the two-dimensional WiggleZ power spectrum. In the joint fit with the other galaxy survey constraints, the reduction in information about r_s compared to the BAO-only BOSS and WiggleZ analyses leads to a broadening of constraints in the direction roughly perpendicular to the BAO-only BOSS contours (Figure 1). Using the Blake et al. (2012) and Chuang et al. (2013) results does, however, lead to tighter constraints on the parameters of most interest in this analysis – Ω_m and w, when it is free - partially breaking the degeneracy apparent in the BAO-only contours.

The LSS Λ CDM constraint of $\Omega_m = 0.290 \pm 0.019$ is around

http://pla.esac.esa.int/pla/aio/planckResults.jsp?

50 per cent weaker than that from current CMB data; it is worth pointing out, though, that it is comparable or stronger than any pre-Planck CMB measurement – the WMAP-9 68 per cent uncertainty on Ω_m is 0.025, while that from combining WMAP-9 with SPT data is 0.019 (Calabrese et al. 2013), for example. It is realistic to expect LSS to constrain Ω_m with comparable precision to Planck in the fairly near future.

The χ^2 value corresponding to the maximum likelihood from the BAO-only ACDM chain is 1.73. We are fitting to a total of 9 data points with two parameters (Ω_m and $H_0 r_s$); the probability for χ^2 per degree of freedom (dof) to exceed the measured value (PTE) is very high - 0.97. This issue is exacerbated in the fit including the additional LSS data: we find $\chi^2/\mathrm{dof} = 3.5/(17-4)$ (PTE of 0.995). The high PTE values remain if we remove the Ly- α constraint and our associated non-Gaussian likelihood. Our analysis neglects interdependence between constraints from different surveys. There is partial overlap in both redshift and sky coverage for WiggleZ and BOSS (see Figure 1 of Drinkwater et al. 2010 and Figure 1 of Ahn et al. 2012), however 70% of the BOSS sky coverage lies outside the WiggleZ regions, and these surveys use somewhat different galaxy selection criteria. We have confirmed that the high PTE remains even if we repeat our fits omitting the constraints from one of these two surveys.

It seems plausible that uncertainties on derived quantities used in this work, such as D_V/r_s and $f\sigma_8$, may be overestimated as a result of individual analyses conservatively choosing methodology approaches that lead to the broadest constraints. Chuang et al. (2012) found that estimating LSS clustering bandpower covariance using lognormal realizations to approximate non-linearities in the density field (Coles & Jones 1991; Percival et al. 2004), rather than N-body simulations, leads to systematically larger uncertainties. This could contribute to the high PTE in the case of the WiggleZ and 6dFGS data, where the lognormal method was used (Blake et al. 2011a; Beutler et al. 2011). We therefore expect the issue of high PTE to be largely resolved through a combination of fitting directly to correlation function or power spectrum measurements, and future improvements in LSS analysis methodology.

4.2 wCDM

For wCDM, the BAO position measurements alone constrain $w=-1.06^{+0.33}_{-0.32},\,\Omega_m=0.292^{+0.045}_{-0.040},\,{\rm and}\,\,H_0\,r_s=(1.045\pm0.058)\times10^4$ km s⁻¹. Addition of the clustering shape, AP and growth rate constraints tighten wCDM constraints, although not to the extent that they did for Λ CDM, with the w constraint improving to -1.14 ± 0.19 . The χ^2 for the LSS wCDM fit is improved by 0.3 compared to Λ CDM; currently, there is no significant evidence for departures from Λ -acceleration from LSS data. The BAO and LSS data constraints on other parameters are fairly robust to allowing freedom in w, while the CMB constraints are significantly broadened. The CMB data exhibit a mild ($\sim1.5\sigma$) preference for w<-1, which leads to shifts in the other parameters shown in Table 2, since these parameters are highly correlated with w when constrained with the CMB alone (see Figure 21 of Planck Collaboration XVI 2013).

Chuang et al. (2013) found that including growth rate measurements improved constraints on w in a joint fit using the BOSS CMASS sample and CMB data. It is worth noting here that, in our fit to the LSS clustering data only, the growth rate measurements effectively only constrain σ_8 , and contribute minimally to constraints on Ω_m or w. This is because $f\sigma_8$ depends weakly on redshift for z < 1 and so there is little leverage for current growth rate measurements.

Table 2. Cosmological constraints from BAO position only (using constraints from top part of Table 1), BAO position plus a baryon density prior from estimation of the primordial deuterium abundance (Section 5.1), LSS clustering (bottom part of Table 1), and the latest CMB measurements (*Planck* temperature and lensing power spectra plus *WMAP* polarization and ACT and SPT small-scale temperature power spectra; Planck Collaboration XVI 2013). We show 68.3 per cent confidence intervals for all parameters and additionally show 95.5 per cent confidence intervals for w.

Model	Parameter	BAO-only	BAO+ $\Omega_b h^2$	LSS	CMB-only
ΛCDM	$\begin{array}{l} \Omega_m \\ H_0 r_s / 10^4 \mathrm{km s^{-1}} \\ H_0 / \mathrm{km s^{-1} Mpc^{-1}} \\ \sigma_8 \end{array}$	0.304 ± 0.040 1.035 ± 0.024 -	$0.308^{+0.040}_{-0.041}$ 1.033 ± 0.024 68.9 ± 3.0	0.290 ± 0.019 1.048 ± 0.022 67.5 ± 2.8 0.802 ± 0.047	$0.307 \pm 0.013 \\ 1.027^{+0.018}_{-0.017} \\ 67.9 \pm 1.0 \\ 0.8233 \pm 0.0097$
wCDM	$\begin{array}{c} w \\ \Omega_m \\ H_0 r_s / 10^4 \mathrm{km s^{-1}} \\ H_0 / \mathrm{km s^{-1} Mpc^{-1}} \\ \sigma_8 \end{array}$	$\begin{array}{c} -1.06^{+0.33}_{-0.32}^{+0.63}_{-0.32}^{+0.045}_{-0.72} \\ 0.292^{+0.045}_{-0.040} \\ 1.045 \pm 0.058 \\ - \\ - \end{array}$	$\begin{array}{c} -1.11^{+0.32}_{-0.32}^{+0.61}_{-0.32}^{+0.041}_{-0.71}\\ 0.299^{+0.042}_{-0.040}\\ 1.050\pm0.057\\ 70.7\pm7.7\\ -\end{array}$	$\begin{array}{c} -1.14^{+0.19}_{-0.19} + 0.36 \\ -0.19^{-0.42} \\ 0.275^{+0.039}_{-0.029} \\ 1.076 \pm 0.045 \\ 70.1 \pm 4.8 \\ 0.77 \pm 0.07 \end{array}$	$\begin{array}{c} -1.49^{+0.30}_{-0.29}^{+0.30}_{-0.29}^{+0.62}\\ 0.204^{+0.052}_{-0.051}\\ 1.287^{+0.219}_{-0.166}\\ 85.0\pm10.9\\ 0.96\pm0.08 \end{array}$

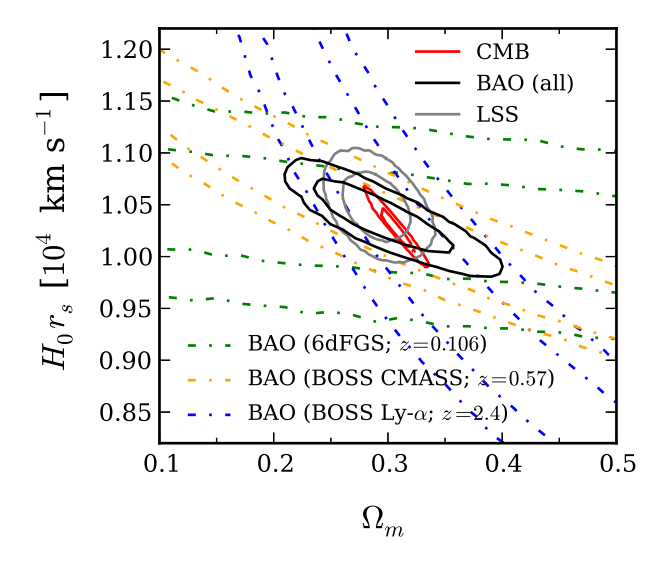


Figure 1. Λ CDM constraints from measurements of BAO position. We show 68.3 and 95.5 per cent confidence contours for the combined BAO data set (Table 1, top), and for the 6dFGS (Beutler et al. 2011), BOSS CMASS (Anderson et al. 2013) and BOSS Ly- α (Slosar et al. 2013) data separately, to illustrate their complementarity. Constraints from our expanded analysis including other large-scale structure clustering constraints (Table 1, bottom), and CMB constraints from combining *Planck*, *WMAP*, ACT and SPT data (Planck Collaboration XVI 2013) are also shown. The BAO, LSS and CMB constraints are in good agreement for the Λ CDM model.

surements to improve expansion history constraints in the absence of an external constraint on σ_8 . In Section 5.2, we show that the growth rate σ_8 constraint does, however, play an important role when assessing the extent to which allowing $w \neq -1$ can relieve tension between the CMB and low-redshift data sets.

5 DISCUSSION

5.1 Comparison with distance ladder H_0 measurements

Figure 2 compares marginalized constraints on H_0 . We show the local distance ladder measurements of $H_0=(73.8\pm2.4)~{\rm km~s^{-1}~Mpc^{-1}}$ measured using Cepheid variable stars and

low-redshift type IA SNe observed with the *Hubble Space Telescope* (HST) by Riess et al. (2011). Similar results were obtained from a more recent re-analysis of HST Cepheid and SNe data using a new estimate of the distance to the Large Magellanic Cloud calibrated using $3.6~\mu m$ observations (Freedman et al. 2012).

The BAO position measurements alone do not provide any H_0 constraint, being sensitive only to the combination $H_0 r_s$. In addition to H_0 and Ω_m , the sound horizon depends on the physical baryon density, $\Omega_b h^2$, though only weakly $-r_s \propto (\Omega_b h^2)^{-0.13}$ for the cosmological models considered here. We are therefore able to obtain constraints on H_0 from the BAO position measurements with the addition of a prior on the baryon density (and the CMB mean temperature, which determines the energy density in radiation, and which we hold fixed to 2.72548 K; Fixsen 2009). The most precise constraints on the baryon density outside the CMB come from estimates of the primordial deuterium abundance from metal-poor damped Ly- α systems. Recently, Pettini & Cooke (2012) found $\Omega_b h^2 = 0.0223 \pm 0.0009$ (assuming no non-standard relativistic species) for a system particularly well-suited to this measurement at $z \sim 3$. Adopting this constraint as a Gaussian prior and repeating the fit to the BAO data in the top part of Table 1 using the parameter set $\{\Omega_m, \Omega_b h^2, H_0\}$, yields $H_0 = 68.9 \pm 3.0 \text{ km s}^{-1} \text{ Mpc}^{-1}$. Alternatively, using a weak CMB-based prior of $\Omega_b h^2 = 0.02218 \pm 0.00130$, five times wider than the CMB-only 68 per cent confidence constraint from Planck Collaboration XVI (2013), gives $H_0 = 68.8 \pm$ 3.1 km s⁻¹ Mpc⁻¹. These values are in good agreement with the LSS clustering constraint and lower by around 1.3σ than the Riess et al. (2011) value. Note that the baryon density is determined from the CMB power spectrum largely through the relative heights of acoustic peaks, rather than their spacing - this weak CMB-based baryon density prior is highly robust to modifications that could alter the acoustic scale, such as extra relativistic species.

It should be noted that the Ly- α data dominate the H_0 constraint in the BAO position plus baryon density fit; removing this data point, we find $H_0=70.1\pm7.1~{\rm km~s^{-1}~Mpc^{-1}}$ for the deuterium abundance $\Omega_b h^2$ prior. The high-redshift information partially breaks degeneracies present in the low-redshift constraints (Figure 1). Using the Busca et al. (2013) Ly- α constraint of $\alpha_r^{-1}=0.954\pm0.077$ (for their method 2 and broadband parametrization of their equation 24), rather than that of Slosar et al. (2013), gives $H_0=66.8\pm3.7~{\rm km~s^{-1}~Mpc^{-1}}$. On the other hand, using the isotropic Ly- α constraint from Slosar et al. (2013), rather than simply the measurement in the radial direction, and assuming

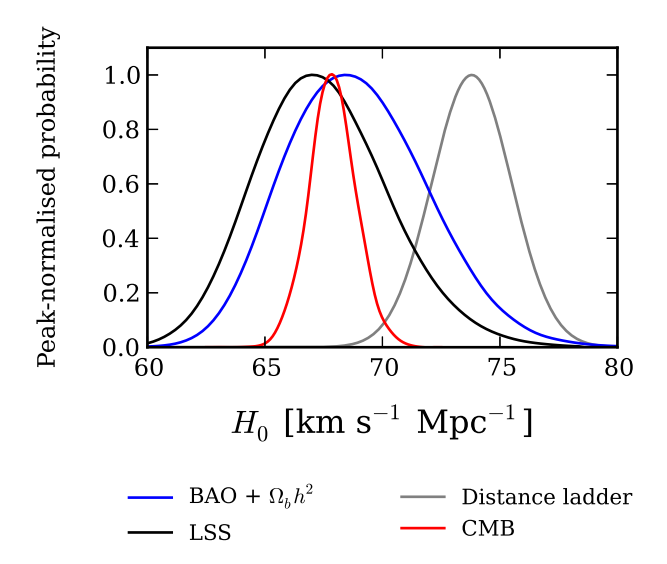


Figure 2. Marginalized H_0 constraints for the Λ CDM model. While BAO position measurements alone do not constraint H_0 , a constraint may be obtained by either adding information from the shape of the large-scale structure correlation function, or adding a prior on the baryon density (here we use the CMB-independent constraint from primordial deuterium abundance estimated by Pettini & Cooke 2012). In either case, there is a mild preference for a lower H_0 value than the distance ladder measurements, consistent with recent *Planck* results. Note that the choice of large-scale structure constraints moderately affects this comparison (see text).

the isotropic distortion parameter $\alpha_{\rm iso} \propto D_A^{0.2} H^{-0.8}$ (Busca et al. 2013), we find $H_0 = 69.2 \pm 2.3 \ {\rm km \ s^{-1} \ Mpc^{-1}}$.

In the expanded LSS clustering analysis, H_0 is constrained from the shape of the galaxy correlation function, which is sensitive to $\Omega_m h^2$. The resulting $\Lambda {\rm CDM}$ constraint of $67.5 \pm 2.8~{\rm km~s^{-1}~Mpc^{-1}}$ is in mild (1.7σ) tension with the direct H_0 measurement. The choice of which galaxy clustering constraints to rely on has some effect here; adding the constraint on $\Omega_m h^2$ from the $z_{\rm eff}=0.35~{\rm SDSS}$ sample from Chuang & Wang (2013), which was not included in our base LSS fit (Section 3), shifts the H_0 constraint to $66.5 \pm 2.1~{\rm km~s^{-1}~Mpc^{-1}}$, which is in tension with the Riess et al. (2011) measurement at around the 2.2σ level, while remaining in good agreement with the CMB value.

Overall, then, we find that the LSS clustering data exhibit qualitatively the same tension with the distance ladder H_0 measurements, assuming a Λ CDM model, as the *Planck* data, preferring a lower H_0 value, although only at fairly weak statistical significance. Clearly, this difference could be largely, or solely, the result of statistical fluctuation. We also discuss the extent to which allowing $w \neq -1$ relieves this, and other, Λ CDM tensions in Section 5.2, below. Discussion of other extensions, such as increasing the number of effective neutrino species, is deferred to future work.

Due to the weak dependence of the sound horizon on the baryon density, the uncertainties given in this section are largely limited by statistical uncertainties in the BAO and LSS clustering data. There is therefore scope for considerable improvement in (model-dependent) H_0 constraints with future LSS clustering data, particularly at high redshift, with minimal dependence on the CMB measurement of the acoustic scale.

5.2 Comparison with type IA supernovae measurements and allowing $w \neq -1$

Measurements of type IA supernovae brightness as a function of redshift constrain the expansion history, and thus Ω_m and w, if an empirical correlation between luminosity and light curve shape is assumed (for discussion of the role of SNe as DE probes, see Weinberg et al. 2012, and references therein). These constraints can be directly compared to those from the BAO position and LSS clustering data. In this work, we compare to the Supernova Legacy Survey (SNLS) compilation, consisting of 472 SNe from various surveys, and analysed by Conley et al. (2011), with marginalization over nuisance parameters relating to known SNe systematic uncertainties

For the Λ CDM model, the SNLS compilation gives $\Omega_m = 0.232 \pm 0.039$ (68 per cent confidence). This is in agreement with, though around 1.3σ lower than, the BAO or LSS constraints of 0.304 ± 0.040 and 0.290 ± 0.019 , respectively. As with H_0 , BAO and LSS constraints on Ω_m are expected to improve significantly in the relatively near future (Section 5.4).

It is interesting to consider the combined LSS, SNe, distance ladder and CMB data in the context of the wCDM model. Taking all quoted uncertainties at face value, combining either the SNLS SNe or distance ladder measurements with CMB data leads to a preference for w<-1 at 2σ (95 per cent confidence limits of $w=-1.13^{+0.13}_{-0.14}$, and $w=-1.24^{+0.18}_{-0.19}$, respectively; Planck Collaboration XVI 2013). If we consider two-dimensional contour plots from the triplet of parameters $\{w,\Omega_m,H_0\}$, a value of $w\simeq-1.2$, with $\Omega_m\simeq0.26$ and $H_0\simeq73$ km s⁻¹ Mpc⁻¹, appears to effectively relieve the tension in the combined data set (Figure 3). For both the CMB and LSS, w and Ω_m are positively correlated, and w and H_0 are anti-correlated. Thus, allowing w<-1 both increases H_0 , improving agreement with the distance ladder measurements, and decreases Ω_m , improving agreement with the SNe.

The situation changes somewhat when we consider LSS growth rate constraints on σ_8 with w free. In Figure 4, we show constraints in the $w-\sigma_8$ plane. In order to include distance ladder and SNe constraints in this comparison, we used the publicly available *Planck* CMB plus SNLS MCMC chain that was importance sampled with the Riess et al. (2011) H_0 prior, having established that there is statistical agreement between the CMB, SNe and distance ladder data in the wCDM model (Figure 3).

Decreasing w below -1 quickly leads to tension between the LSS and CMB determinations of σ_8 , which are in good agreement for Λ CDM – see Table 2. Consequently, when the constraints on σ_8 from the growth rate measurements are considered, allowing w < -1 appears less effective at relieving tension in the combined CMB, LSS, distance ladder and SNe data set.

It is worth examining why the CMB and LSS contours in Figure 4 are roughly orthogonal. For the flat wCDM model, the constraints on w, Ω_m and H_0 from the CMB are driven by the requirements that the angular diameter distance to last scattering, and the physical matter density, $\Omega_m h^2$, remain roughly fixed. This is achieved via the contours shown in Figure 3, and for w < -1 leads to a universe with a lower fractional matter density at the present time than inferred for w = -1. The dominant effect for σ_8 is an increase in H_0 , which means σ_8 corresponds to rms mass fluctuations in smaller spheres (by definition, σ_8 is the rms fluctuation in spheres of radius $8 \ h^{-1}$ Mpc). The CMB prediction for σ_8 is therefore higher for w < -1 than for Λ CDM.

The LSS growth rate measurements probe σ_8 directly though

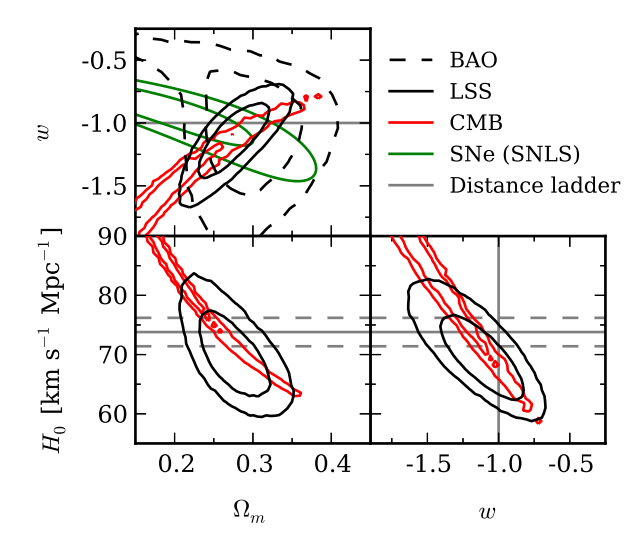


Figure 3. Marginalized two-dimensional constraints from the triplet of parameters $\{w,\Omega_m,H_0\}$ for the wCDM model. We compare results from the BAO and LSS clustering analyses in this work with the latest CMB constraints (Planck Collaboration XVI 2013), the SNLS SNe compilation (Conley et al. 2011), and local distance ladder H_0 measurements (Riess et al. 2011). Decreasing w below -1 appears to relieve the ΛCDM tension between these data sets when these three parameters are considered – but see Figure 4.

 $f\sigma_8$, which depends on the growing mode δ as

$$f(z)\sigma_8(z) = \frac{d\ln\delta}{d\ln a} \frac{\delta(z)}{\delta(0)} \sigma_8$$

= $-\frac{1+z}{\delta(0)} \frac{d\delta}{dz} \sigma_8$. (8)

If w<-1, the expansion history measured by current BAO and AP data can be recovered by decreasing Ω_m , as for the CMB (Figure 3). At $z\sim0.6$, where the growth rate constraints are strongest, the dominant effect is an increase in $(-d\delta/dz)$, and, consequently, a decrease in σ_8 to balance the right-hand side of equation (8).

We can quantitatively assess the contribution of the growth rate constraints by importance sampling (e.g. Lewis & Bridle 2002) the CMB plus BAO chain supplied by the *Planck* collaboration. We modify the chain sample weights using the ratio of the LSS likelihood adopted in this work to the BAO-only likelihood adopted by Planck Collaboration XVI (2013), which used the BAO constraints from 6dFGS, SDSS and BOSS (CMASS). We find a constraint of

$$w = -1.03^{+0.06}_{-0.06}{}^{+0.12}_{-0.12}$$
 (CMB+LSS; 68 and 95 per cent confidence), (9)

which is around 30 per cent tighter than in the original chain ($w=-1.08^{+0.09}_{-0.09}^{+0.18}$). There are correspondingly tight constraints on other parameters, which are in good agreement with the Λ CDM values in Table 2: we find $H_0=(68.9\pm1.7)~{\rm km~s^{-1}~Mpc^{-1}},$ $\Omega_m=0.297\pm0.015$ and $\sigma_8=0.829\pm0.018$. We expect importance sampling the CMB plus BAO chain to be a reasonable approximation to running a full chain with the LSS constraints included, since the wCDM degeneracies in the CMB data are already largely broken with the BAO data.

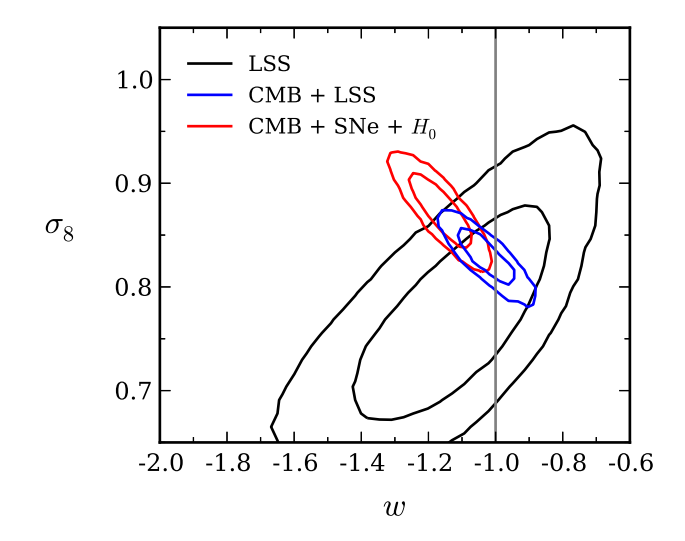


Figure 4. Marginalized σ_8 and w constraints (68.3 and 95.5 per cent confidence) in the wCDM model. While tension in the combined CMB, SNe and distance ladder data set is effectively relieved by allowing w < -1 (Figure 3), the resulting σ_8 constraint is in moderate tension with the large-scale structure growth rate constraints from redshift-space distortion measurements. Note that the CMB and LSS constraints on σ_8 are in good agreement for the Λ CDM model (Table 2); the combined CMB and LSS constraint is $w = -1.03 \pm 0.06$.

5.3 Comparison with cluster counts and weak lensing shear correlation measurements

Incorporating growth rate constraints from redshift-space distortions also allows us to compare the LSS constraints in the $\sigma_8 - \Omega_m$ plane to other low-redshift probes of the amplitude of matter fluctuations, including counts of galaxy clusters and galaxy weak gravitational lensing measurements. This comparison is made in Figure 5 assuming a ΛCDM model, using a pair of recent constraints. We have plotted contours corresponding to $\sigma_8(\Omega_m/0.27)^{0.6} =$ 0.79 ± 0.03 from the weak lensing shear correlation function analysis of data from the Canada-France Hawaii Telescope Lensing Survey (CFHTLens; Kilbinger et al. 2013), and $\sigma_8(\Omega_m/0.29)^{0.322} =$ 0.775 ± 0.010 from a cosmological analysis of clusters selected by the thermal Sunyaev Zel'dovich (SZ) effect using Planck (Planck Collaboration XX 2013). We do not see any degree of tension between the LSS clustering and other data sets here, although there is clearly some tension between the CMB power spectrum data and the weak lensing and cluster count constraints (see also Sections 5.5.2 and 5.5.3 of Planck Collaboration XVI 2013).

There is minimal correlation between σ_8 and Ω_m from current LSS data; making a more meaningful comparison using LSS clustering essentially requires tighter constraints on the growth rate to better measure σ_8 .

5.4 Future data

The Ly- α data are a powerful complement to the galaxy clustering measurements at lower redshift. Without the BOSS Ly- α point, errors on Ω_m are more-than doubled for the BAO-only Λ CDM model, and tripled for wCDM. Constraints on w itself are also greatly degraded, such that w is almost unconstrained from below. When additional LSS constraints are included, the relative impor-

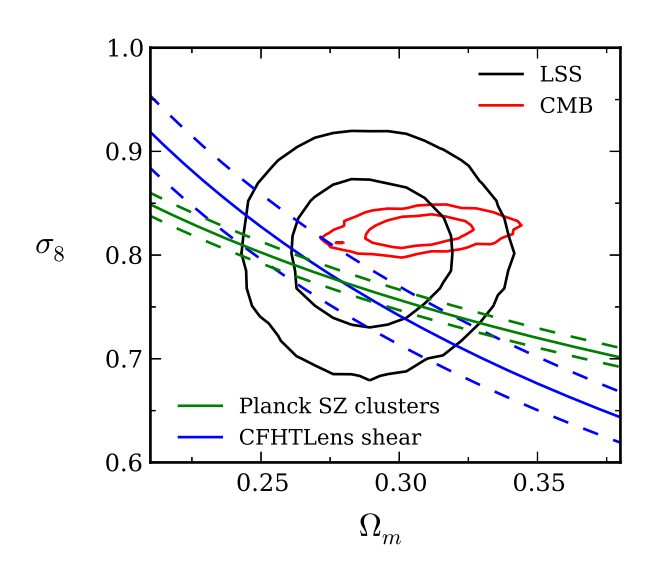


Figure 5. Comparison of Λ CDM constraints (68.3 and 95.5 per cent confidence) in the $\sigma_8-\Omega_m$ plane for CMB and several low-redshift data sets. While growth rate information from redshift-space distortions allows LSS clustering measurements to constrain σ_8 , current precision is too low to meaningfully inform the comparison of CMB constraints with those from (for instance) cluster abundance (Planck Collaboration XX 2013) or weak lensing shear correlations (Kilbinger et al. 2013).

tance of the Ly- α constraint is diminished; removing the Ly- α constrain degrades the LSS w constraint by around 15 per cent, from -1.14 ± 0.19 to -1.18 ± 0.22 . Given that the Ly- α BAO constraints rely on analysis methodology less mature than used for the galaxy clustering measurements, it is encouraging that the shift in mean w value from removing the Ly- α constraint is small compared to uncertainties.

As mentioned in Section 1, the quality and quantity of BAO position and LSS clustering data will improve considerably in coming months and years. The BOSS survey is expected to provide spectroscopic detections of roughly three times more galaxies than in the DR9 release, and around 50 per cent more quasars, leading to significant improvements over the constraints used in our analysis, particularly for the Ly- α BAO measurements (Schlegel et al. 2009). Various upcoming surveys are targeting BAO in the z>1 universe, including the Dark Energy Survey (The Dark Energy Survey Collaboration 2005), MS-DESI, HET-DEX 5 (Hill et al. 2009) and, looking further ahead, WFIRST 6 and Euclid 7 (Amendola et al. 2012). Many of these experiments will also attempt to constrain DE in other ways, using type IA SNe, galaxy weak lensing and cluster abundance, for example.

Telescopes including the Canadian HI Intensity Mapping Experiment⁸ (CHIME), currently under construction in western Canada, plan to measure high-redshift BAO using HI intensity fluctuations. If the Galactic synchrotron foreground can be removed, CHIME has the potential to cheaply and quickly yield very competitive DE constraints from a diffuse tracer of LSS.

We also note that BAO constraints at low redshift ($z \lesssim 0.2$), from surveys such as WALLABY⁹ and TAIPAN, would significantly improve on constraints from the 6dFGS (Beutler et al. 2011). Amongst other things, these data would yield strong constraints on H_0 through an approach like that discussed in Section 5.1, when combined with high-redshift information.

We have highlighted the usefulness of growth rate constraints in both improving DE constraints and assessing consistency between data sets (Sections 5.2 and 5.3). There are also good prospects for future improvement in these measurements (e.g. Weinberg et al. 2012).

Our analysis of current LSS constraints demonstrates that we are already able to make meaningful comparisons between low-redshift data even without strong priors from the high-redshift universe probed by the CMB. It seems likely, if not inevitable, that future Λ CDM tensions between different cosmological probes will continue to arise as new data become available and constraints become more precise. Even if such tensions do not end up being ascribed to new physics, we must put ourselves in a position to make that assessment as robustly as possible. Examining different combinations of low-redshift data with and without CMB constraints should be a useful part of this process.

6 CONCLUSIONS

We have performed joint fits of cosmological parameters to current BAO position and LSS clustering measurements. We have shown that the BAO and LSS data are now of sufficiently high precision to make useful comparisons with other low-redshift cosmological probes in the virtual absence of CMB anisotropy constraints. We find that the BAO and LSS constraints are in good agreement with the latest CMB results from *Planck* for the Λ CDM model, and mildly prefer a lower value of H_0 , and higher value of Ω_m , than some recent local distance ladder and type IA SNe measurements (Sections 5.1 and 5.2).

We note that the Λ CDM tension between Planck, distance ladder and SNe data reported by Planck Collaboration XVI (2013) appears to be effectively relieved by allowing w<-1, and that the CMB and LSS clustering data separately tolerate such behaviour. We show that the growth rate constraint on σ_8 from redshift-space distortions, is, however, in some tension with the combined CMB, distance ladder and SNe constraint in the wCDM model. Combining CMB, BAO and LSS data, including the growth rate information, we find $w=-1.03\pm0.06$; this constraint is around 30 per cent tighter than for CMB plus BAO position only, and completely consistent with Λ CDM.

GA acknowledges support from a Canadian Institute for Theoretical Astrophysics (CITA) National Fellowship. This work was also supported by the Natural Sciences and Engineering Research Council of Canada (NSERC) and the Canadian Institute for Advanced Research (CIFAR). The authors would like to thank Chris Blake, Nicolás Busca, Chia-Hsun Chuang and Will Percival for clarification regarding the BAO and LSS measurements, Wendy Freedman for information relating to the distance ladder H_0 measurements, and Alex Conley for providing likelihood contours from the Conley et al. (2011) SNLS analysis. We also thank the referee for useful comments and suggestions.

⁴ http://www.darkenergysurvey.org/

⁵ http://hetdex.org/

⁶ http://wfirst.gsfc.nasa.gov/science/de/

⁷ http://sci.esa.int/science-e/www/area/index.cfm?fareaid=102

⁸ http://chime.phas.ubc.ca/

⁹ http://www.atnf.csiro.au/research/WALLABY/

REFERENCES

Ahn C. P. et al., 2012, ApJS, 203, 21

Akeret J., Seehars S., Amara A., Refregier A., Csillaghy A., 2012, preprint (arXiv:1212.1721)

Albrecht A. et al., 2006, preprint (arXiv:0609591)

Alcock C., Paczynski B., 1979, Nature, 281, 358

Amendola L. et al., 2012, preprint (arXiv:1206.1225)

Anderson L. et al., 2013, preprint (arXiv:1303.4666)

Anderson L. et al., 2012, MNRAS, 427, 3435

Ballinger W. E., Peacock J. A., Heavens A. F., 1996, MNRAS, 282, 877

Bennett C. L. et al., 2012, preprint (arXiv:1212.5225)

Beutler F. et al., 2011, MNRAS, 416, 3017

Beutler F. et al., 2012, MNRAS, 423, 3430

Blake C. et al., 2012, MNRAS, 425, 405

Blake C. et al., 2011a, MNRAS, 415, 2892

Blake C. et al., 2011b, MNRAS, 418, 1725

Blake C. et al., 2011c, MNRAS, 418, 1707

Busca N. G. et al., 2013, A&A, 552, A96

Calabrese E. et al., 2013, Phys. Rev. D, 87, 103012

Chevallier M., Polarski D., 2001, Int. J. Mod. Phys., D10, 213

Chuang C.-H. et al., 2013, MNRAS, 433, 3559

Chuang C.-H., Wang Y., 2013, MNRAS

Chuang C.-H., Wang Y., Hemantha M. D. P., 2012, MNRAS, 423, 1474

Cole S. et al., 2005, MNRAS, 362, 505

Coles P., Jones B., 1991, MNRAS, 248, 1

Conley A. et al., 2011, ApJS, 192, 1

Das S. et al., 2013, preprint (arXiv:1301.1037)

de la Torre S. et al., 2013, A&A, 557, A54

Drinkwater M. J. et al., 2010, MNRAS, 401, 1429

Dunkley J., Bucher M., Ferreira P. G., Moodley K., Skordis C., 2005, MN-RAS, 356, 925

Eisenstein D. J., Hu W., 1998, ApJ, 496, 605

Eisenstein D. J., Hu W., Tegmark M., 1998, ApJ, 504, L57

Eisenstein D. J., Seo H.-J., Sirko E., Spergel D. N., 2007a, ApJ, 664, 675

Eisenstein D. J., Seo H.-J., White M., 2007b, ApJ, 664, 660

Eisenstein D. J. et al., 2005, ApJ, 633, 560

Fixsen D. J., 2009, ApJ, 707, 916

Foreman-Mackey D., Hogg D. W., Lang D., Goodman J., 2013, PASP, 125, 306

Freedman W. L., Madore B. F., Scowcroft V., Burns C., Monson A., Persson S. E., Seibert M., Rigby J., 2012, ApJ, 758, 24

Goodman J., Weare J., 2010, Comm. App. Math. Comp. Sci., 5, 65

Guzzo L. et al., 2008, Nature, 451, 541

Hawkins E. et al., 2003, MNRAS, 346, 78

Hill R. S. et al., 2009, ApJS, 180, 246

Hinshaw G. et al., 2012, preprint (arXiv:1212.5226)

Hou Z. et al., 2012, preprint (arXiv:1212.6267)

Hu W., Sugiyama N., 1996, ApJ, 471, 542

Kaiser N., 1987, MNRAS, 227, 1

Kilbinger M. et al., 2013, MNRAS, 430, 2200

Komatsu E. et al., 2011, ApJS, 192, 18

Lewis A., Bridle S., 2002, Phys. Rev. D, 66, 103511

Lewis A., Challinor A., Lasenby A., 2000, ApJ, 538, 473

Linder E. V., 2003, Phys. Rev. Lett., 90, 091301

Metropolis N., Rosenbluth A. W., Rosenbluth, M. N. and Teller A. H., 1953, J. Chem. Phys., 21, 1087

Padmanabhan N., Xu X., Eisenstein D. J., Scalzo R., Cuesta A. J., Mehta K. T., Kazin E., 2012, MNRAS, 427, 2132

Peebles P. J. E., Yu J. T., 1970, ApJ, 162, 815

Percival W. J. et al., 2004, MNRAS, 353, 1201

Percival W. J. et al., 2010, MNRAS, 401, 2148

Pettini M., Cooke R., 2012, MNRAS, 425, 2477

Planck Collaboration XV, 2013, preprint (arXiv:1303.5075)

Planck Collaboration XVI, 2013, preprint (arXiv:1303.5076)

Planck Collaboration XVII, 2013, preprint (arXiv:1303.5077)

Planck Collaboration XX, 2013, preprint (arXiv:1303.5080)

Reichardt C. L. et al., 2012, ApJ, 755, 70

Reid B. A. et al., 2010, MNRAS, 404, 60

Riess A. G. et al., 2011, ApJ, 730, 119

Ross N. P. et al., 2007, MNRAS, 381, 573

Samushia L., Percival W. J., Raccanelli A., 2012, MNRAS, 420, 2102

Sánchez A. G., Baugh C. M., Angulo R. E., 2008, MNRAS, 390, 1470

Sánchez A. G. et al., 2013, MNRAS, 433, 1202

Schlegel D., White M., Eisenstein D., 2009, in ArXiv Astrophysics eprints, Vol. 2010, astro2010: The Astronomy and Astrophysics Decadal Survey, p. 314

Shoji M., Jeong D., Komatsu E., 2009, ApJ, 693, 1404

Sievers J. L. et al., 2013, preprint (arXiv:1301.0824)

Silveira V., Waga I., 1994, Phys. Rev. D, 50, 4890

Slosar A. et al., 2013, J. Cosmology Astropart. Phys., 4, 26

Story K. T. et al., 2012, preprint (arXiv:1210.7231)

Tegmark M., 1997, Phys. Rev. D, 55, 5895

The Dark Energy Survey Collaboration, 2005, preprint (arXiv:0510346)

Weinberg D. H., Mortonson M. J., Eisenstein D. J., Hirata C., Riess A. G., Rozo E., 2012, preprint (arXiv:1201.2434)

Xu X., Cuesta A. J., Padmanabhan N., Eisenstein D. J., McBride C. K., 2013, MNRAS, 431, 2834